Available online at www.sciencedirect.com
ScienceDirect
Acta Materialia 56 (2008) 3777–3785
Acta MATERIALIA
www.elsevier.com/locate/actamat

# Room-temperature creep and structural relaxation of Mg–Cu–Y metallic glasses

A. Castellero [a,1], B. Moser [b,2], D.I. Uhlenhaut [a], F.H. Dalla Torre [a], J.F. Löffler [a,*]

[a] *Laboratory of Metal Physics and Technology, Department of Materials, ETH Zurich, Wolfgang-Pauli-Strasse 10, 8093 Zurich, Switzerland*
[b] *EMPA Materials Science and Technology, Feuerwerkerstrasse 39, 3602 Thun, Switzerland*

Received 12 February 2008; received in revised form 28 March 2008; accepted 8 April 2008
Available online 16 May 2008

**Abstract**

Structural relaxation of Mg–Cu–Y metallic glasses occurs at room-temperature (~0.7 $T_g$) and induces an abrupt embrittlement after periods of time that depend on the relative proportions of Cu and Mg. Internal friction measurements of as-quenched samples show that $Mg_{65}Cu_{25}Y_{10}$ is in a more relaxed state than $Mg_{85}Cu_5Y_{10}$, suggesting a more compact structure for the alloy with a larger amount of Cu, which is the smallest atom in the system. Relaxation spectra, calculated from the anelastic component of nanoindentation creep curves, show that the two alloys are in a similar relaxed state, when they become brittle. The results are discussed in terms of the defects characterizing the disordered structure of the metallic glass.


*Keywords:* Metallic glasses; Magnesium; Nanoindentation; Creep test; Structural relaxation

## 1. Introduction

It is well known that metallic glasses, or amorphous alloys, can lie in different energy levels (also called isoconfigurational states) depending on the number of structural defects frozen in the sample during quenching (for a review see Ref. [1]). In fact, higher cooling rates lead to a higher degree of metastability (i.e., higher number of structural defects), while lower cooling rates result in a more relaxed state in the metallic glass. Lower energy levels can be accessed by annealing below the glass transition temperature, $T_g$, i.e., by promoting a so-called structural relaxation which makes the structure denser and induces changes in the mechanical, electrical, magnetic, thermal and transport properties. During structural relaxation the frozen-in "defects", which have been described in terms of free volume [2], stress inhomogeneities [3], shear transformation zones [4] and non-coincident atomic sites configurations at intercluster boundaries [5], are progressively annihilated. A fundamental issue affecting potential applications of metallic glasses is the degradation of mechanical properties at various stress levels, such as fracture toughness [6], bending plasticity [7], anelasticity [8] and internal friction [9], caused by structural relaxation.

Metallic glasses are expected to be tough when the size of the plastic zone at the tip of a sharp crack, $d$ (usually <1 mm), is larger than the sample thickness, $t$ [10]. Similarly, a size effect is observed in bending, where the increase of shear band spacing and shear offsets with sample thickness generates easier crack initiation in the shear bands, with consequent crack propagation and failure [11]. The plasticity or brittleness of metallic glasses has also recently been correlated with the value of the Poisson ratio, $\nu$ (or, equivalently, the ratio $G/B$, where $G$ is the shear modulus and $B$ is the bulk modulus) [12–14]: for values of $\nu$ larger than ~0.32 (or $G/B < 0.40$) the shear band tip tends to extend rather than induce crack initiation, allowing

* Corresponding author. Tel.: +41 44 632 2565; fax: 41 44 633 1421.
*E-mail address:* joerg.loeffler@mat.ethz.ch (J.F. Löffler).
[1] Present address: Università di Torino, NIS Centre of Excellence, Dipartimento di Chimica IFM, via P. Giuria 7, I-10125 Torino, Italy.
[2] Present address: Alcan Technology and Management AG, Badische Bahnhofstrasse 16, 8212 Neuhausen, Switzerland.

1359-6454/$34.00 © 2008 Acta Materialia Inc. Published by Elsevier Ltd. All rights reserved.
doi:10.1016/j.actamat.2008.04.021

formation of multiple shear bands and leading to the macroscopic plasticity observed [15].

The reduction in toughness and bending plasticity induced by structural relaxation is caused by the reduction of the plastic zone at the crack tip, which means that the metallic glass loses the ability to blunt a sharp crack, favoring de-cohesion [16]. On the microscopic level this can be explained in terms of a lower number of sites, i.e., weak regions or "defects" in the metallic glass, where shear-induced dilatations can initiate and, eventually, generate a shear band. In other words, the lower nucleation rate of shear bands, which are able to reduce the stress concentration at the crack tip, promotes the propagation of the crack in relaxed metallic glasses [17]. In fact, scanning electron microscopy of impact-tested $Zr_{41.2}Ti_{13.8}Cu_{12.5}$ $Ni_{10.0}Be_{22.5}$ (Vit 1) specimens showed extensive shear banding at the root of the notch in as-cast samples and brittle cleavage-like fracture in the annealed samples [17,18].

In the case of anelasticity, each deformation process may be associated with the activation of typical "defects". It was shown by means of thermal cycling (see e.g. [19,20]) that anelastic deformation and annealing-induced structural relaxation can be separated into reversible and irreversible components. This has been explained in terms of chemical short-range ordering (CSRO) and topological short-range ordering (TSRO), respectively. Such a sharp separation between TSRO and CSRO, criticized by Gibbs and Sinning [21] and Khonik et al. [22], is probably too simple an explanation for such a complex phenomenon, because CSRO is unlikely without an accompanying TSRO.

Stress-induced relaxation (i.e., anelasticity or delayed elasticity) is strongly affected by the degree of structural relaxation in the glass, but does not permanently affect the defect population (e.g., excess volume) in the glass since anelasticity is fully recoverable. However, in structurally relaxed glasses the number of weak regions where the shear transformations may be activated is lower because of the glass densification (i.e., annihilation of defects, independent of the way they are defined) and viscoplastic (permanent) deformation.

The effect of near-$T_g$ structural relaxation on mechanical properties has been studied in the past [1,6–9]. However, the discovery of new alloys with very low $T_g$ (close to room-temperature), such as metallic glasses based on Mg [23] and Ce [24], has initiated new interest in this topic [14,25,26], since structural relaxation induces embrittlement in these alloys even at room-temperature, causing some concern about their potential application.

Here, we investigate the effect of structural relaxation on the mechanical properties of $Mg_{65}Cu_{25}Y_{10}$ and $Mg_{85}Cu_5Y_{10}$ metallic glasses, with particular emphasis on room-temperature embrittlement upon bending and the anelastic/viscoplastic deformation which occurs during nanoindentation creep. The mechanical properties are discussed in terms of defects characterizing the amorphous structure, and also on the basis of results obtained recently [27] via positron annihilation spectroscopy (PAS).

## 2. Experimental methods

The master alloys with nominal composition $Mg_{65}Cu_{25}Y_{10}$ and $Mg_{85}Cu_5Y_{10}$ (compositions are given in at.%) were prepared under a high-purity Ar atmosphere in an induction furnace by mixing elemental Mg and the eutectic compositions $Cu_{25}Y_{10}$ and $Cu_5Y_{10}$, respectively (prepared by arc-melting under high-purity Ar). The elements had a purity ranging from 99.9% (Y) to 99.99% (Cu and Mg). Amorphous foils with a thickness of $50 \pm 2$ μm were prepared by splat-quenching in high-purity Ar. The shiny surface required for the subsequent nanoindentation measurements was obtained by quenching the melt between two well-polished (1/4 μm) Cu plates, since subsequent polishing of the splat-quenched foils would have been too time-consuming for the purpose of studying the early stages of relaxation.

The as-quenched specimens were stored in liquid nitrogen immediately after preparation to avoid room-temperature structural relaxation. The amorphous structure of the as-quenched and relaxed samples was confirmed by X-ray diffraction (XRD) with Cu Kα radiation using a Siemens D5000 diffractometer. The composition of the alloys was checked using an energy dispersion spectroscopy microprobe attached to a CamScan scanning electron microscope: deviations from the nominal compositions were within ±1–2 at.%.

The thin foils were bent between two parallel plates, which were driven towards each other by means of a micrometric screw. The bending strain, $\varepsilon$, was approximated as

$$\varepsilon = \frac{t}{D - t} \tag{1}$$

where $t$ is the thickness of the sample and $D$ is the smallest distance to which the two parallel plates can be moved without breaking the samples. For a fully "ductile" sample the bending strain is 1 (or 100%). The number of measurements performed for each relaxed state was between 7 and 10.

Differential scanning calorimetry (DSC) measurements were run under a flow of high-purity Ar with a Seiko Instruments DSC220CU at a heating rate of 10 K $min^{-1}$. The storage and loss components of the Young's modulus were measured at 10 Hz by dynamic mechanical analysis (DMA) in tension configuration using a Mettler DMA Messmodul apparatus. The storage modulus, $E'$, and loss modulus, $E''$, respectively, represent the solid-like and liquid-like behavior of the glass, and the loss factor $\tan\delta = E''/E'$ is a measure of the ratio between elastic and viscoelastic properties. In purely elastic materials, which show only solid-like behavior, $\tan\delta$ is 0 and the phase shift, $\delta$, is 0°; in fully viscous materials, showing a pure liquid-like behavior, $\tan\delta$ tends to infinity and $\delta$ is 90°. The accuracy of the moduli values depends strongly on the precision

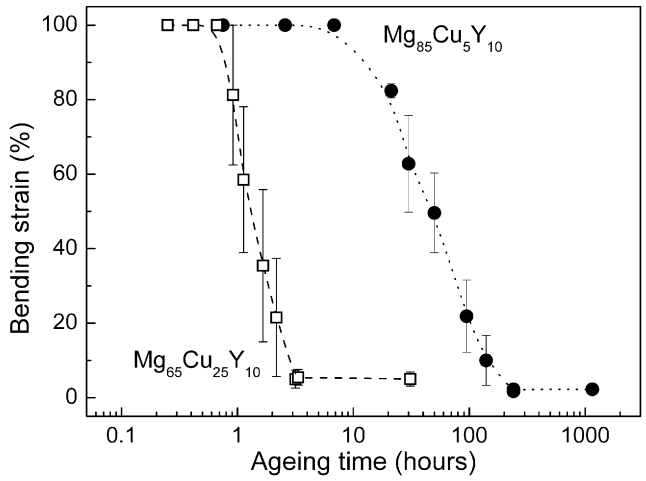


Fig. 1. Bending strain of splat-cooled amorphous $Mg_{65}Cu_{25}Y_{10}$ (open squares) and $Mg_{85}Cu_5Y_{10}$ (full circles) as a function of the ageing time at room-temperature.

Table 1
Glass transition, $T_g$, and crystallization temperatures at different heating rates for $Mg_{65}Cu_{25}Y_{10}$ and $Mg_{85}Cu_5Y_{10}$ metallic glasses

| Alloy | Heating rate (°C min$^{-1}$) | $T_g$ (inflection point) (°C) | $T_{x1}$ (onset) (°C) | $T_{x2}$ (peak) (°C) | References |
|---|---|---|---|---|---|
| $Mg_{65}Cu_{25}Y_{10}$ | 10 | 143 | 195 | 300 | This work |
| | 20 | 147 | 200 | 303 | This work |
| | 20 | 148 | 195 | 290 | [30] |
| | 40 | 152 | 213 | – | [29] |
| $Mg_{85}Cu_5Y_{10}$ | 10 | 153 | 172 | 280 | This work |
| | 40 | 161 | 183 | 288 | This work |
| | 40 | 162 | 190 | – | [29] |

$T_{x1}$ represents the onset of the first crystallization peak; $T_{x2}$ denotes the peak temperature of the second crystallization event.

with which the thickness of the foils can be measured (±2 μm).

Nanoindentation measurements were performed with a Nano XP from MTS Systems Corporation (Eden Prairie, MN) using a Berkovich indenter. Hardness and reduced Young's modulus were evaluated according to the analysis introduced by Oliver and Pharr [28]. Creep measurements were performed according to the following sequence: after loading the samples up to 350 mN at 10 mN s$^{-1}$, the indenter was held at the maximum load for 120 s; after unloading at 10 mN s$^{-1}$, the indenter was kept for another 120 s at 3.5 mN (1% of the maximum load) to let the sample recover the anelastic deformation. At the onset of the ageing process, measurements were averaged in groups of five, and, later on, in groups of 10. The stability of the machine over the whole period of measurement (about 2 weeks) was checked by periodically indenting a reference material (Al).

## 3. Results

Fig. 1 shows the bending strain of $Mg_{65}Cu_{25}Y_{10}$ (open squares) and $Mg_{85}Cu_5Y_{10}$ (full circles), estimated using Eq. (1), as a function of the ageing time at room-temperature. Both alloys show a ductile-to-brittle transition after a critical ageing time which differs for the two compositions.

Table 1 summarizes the thermal properties of $Mg_{65}Cu_{25}Y_{10}$ and $Mg_{85}Cu_5Y_{10}$ obtained by DSC. The glass transition and the crystallization temperatures are in reasonable agreement with previously published data [29,30]. Fig. 2 shows an enlargement of the sub-$T_g$ region for the DSC traces of $Mg_{85}Cu_5Y_{10}$ (a) and $Mg_{65}Cu_{25}Y_{10}$ (b), where the glass transition is clearly preceded by an exothermic signal due to structural relaxation upon heating. Both $Mg_{85}Cu_5Y_{10}$ and $Mg_{65}Cu_{25}Y_{10}$ show, during room-temperature ageing (see arrow direction), a shift of the relaxation peak towards higher temperatures together with a reduction of the enthalpy released during the relaxation. This means that the glasses move progressively towards a more relaxed state characterized by a lower energy level.

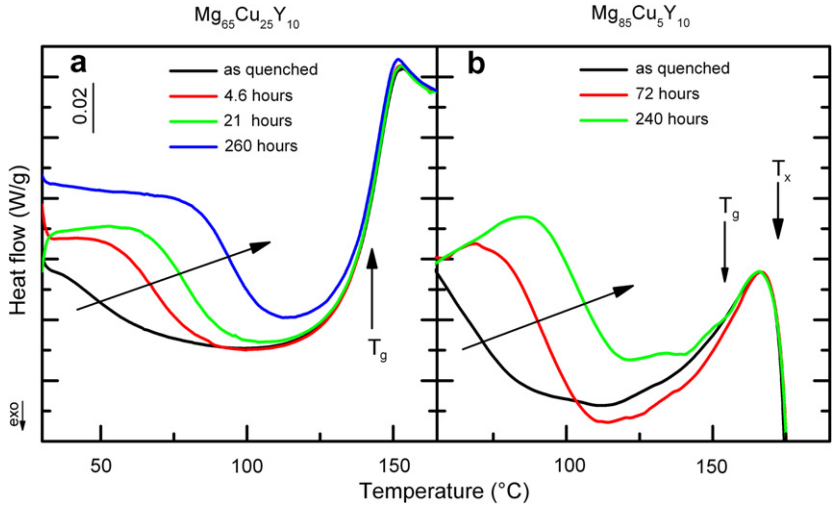


Fig. 2. Relaxation signals in DSC traces at a heating rate of 10 °C min$^{-1}$ for $Mg_{65}Cu_{25}Y_{10}$ (a) and $Mg_{85}Cu_5Y_{10}$ (b) after ageing at room-temperature.

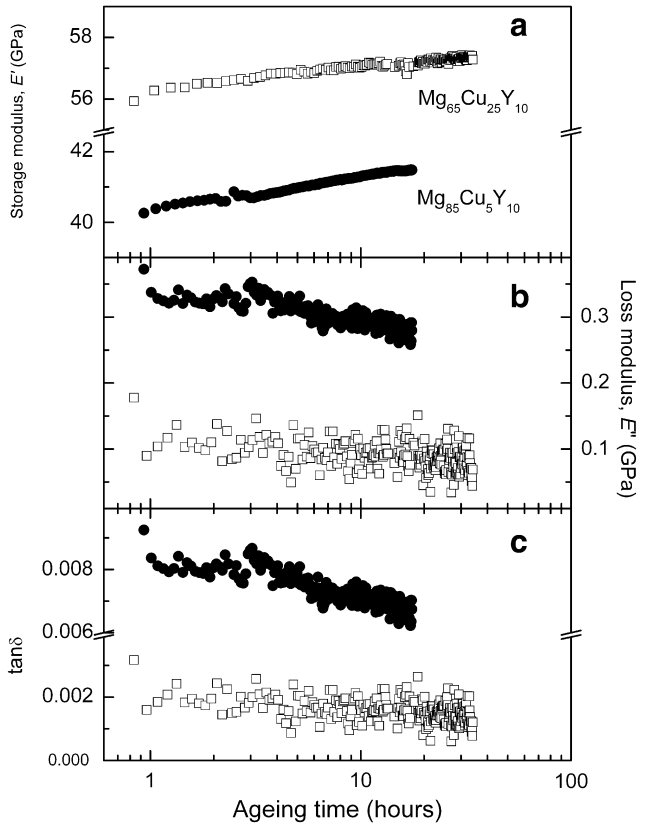


Fig. 3. (a) Storage modulus $E'$ and (b) loss modulus $E''$ measured by DMA in tensile configuration at a frequency of 10 Hz, and (c) calculated internal friction ($\tan\delta$) for $Mg_{65}Cu_{25}Y_{10}$ (open squares) and $Mg_{85}Cu_5Y_{10}$ (full circles) as a function of room-temperature ageing.

Fig. 3a and b shows the storage and loss moduli of $Mg_{65}Cu_{25}Y_{10}$ (open squares) and $Mg_{85}Cu_5Y_{10}$ (full circles) obtained by DMA at 10 Hz as a function of ageing time. The storage modulus, $E'$, increases with ageing time, while the loss modulus, $E''$, decreases. Fig. 3c shows that the loss factor $\tan\delta = E''/E'$ also decreases with ageing. The mean values of $E'$ for $Mg_{65}Cu_{25}Y_{10}$ and $Mg_{85}Cu_5Y_{10}$ are 57 GPa and 41 GPa, respectively. The value of $E'$ for the $Mg_{85}Cu_5Y_{10}$ thin foil accords with those reported in the literature obtained from tensile tests (44 GPa [29]) and resonance frequency and damping analysis (44 GPa [14]) of a $Mg_{85}Cu_5Y_{10}$ ribbon and thin foil, respectively. The variation of about 7% between the values obtained here and those from the literature can be explained by the difficulty of precisely measuring the thickness of thin samples such as ribbons and splat-quenched foils, which generates an error of about ±4% in modulus. The non-negligible difference between our value of $E'$ for $Mg_{65}Cu_{25}Y_{10}$ (57 GPa) and that reported in Ref. [31] (69 GPa) probably results from a different degree of relaxation [32], since our sample was quenched rapidly while that in Ref. [31] was a slowly cooled bulk sample. The Young's modulus estimated as the weighted average of the constituent crystalline elements [33] (57 and 49 GPa for $Mg_{65}Cu_{25}Y_{10}$ and $Mg_{85}Cu_5Y_{10}$, respectively) is also comparable with the experimental values.

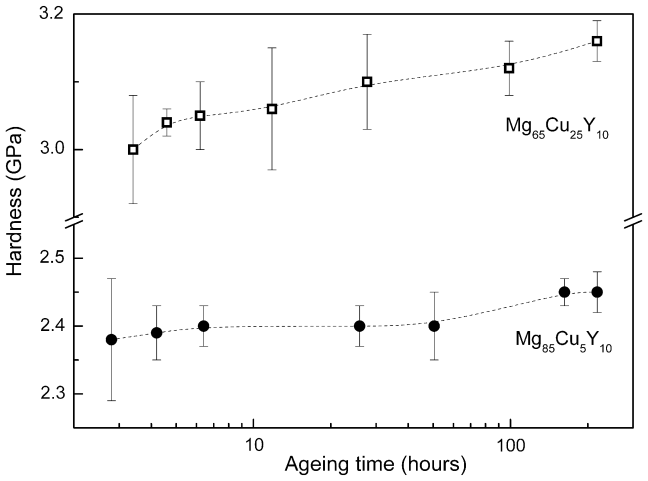


Fig. 4. Nanoindentation hardness of $Mg_{65}Cu_{25}Y_{10}$ (open squares) and $Mg_{85}Cu_5Y_{10}$ (full circles) as a function of room-temperature ageing.

Fig. 4 shows the hardness of the two alloys measured by nanoindentation. Both $Mg_{65}Cu_{25}Y_{10}$ and $Mg_{85}Cu_5Y_{10}$ seem to become progressively harder with ageing time, even if there is a large scatter of the data resulting from the extreme sensitivity of this technique to the local properties of the material.

Fig. 5 shows the experimental raw data for the differently aged Mg-based samples regarding the creep at 350 mN (a and d) and creep recovery at 3.5 mN (b and e). It is clear that not all the deformation induced at 350 mN is recovered at 3.5 mN. The difference between the absolute values of the creep and creep recovery gives the permanent deformation occurring at 350 mN (Fig. 5c and f).

The deformation due to creep, creep recovery (recoverable anelasticity) and permanent viscoplasticity progressively decreases with ageing time, as indicated by the arrows in Fig. 5.

## 4. Discussion

The progressive shift of the relaxation signal to higher temperatures and the reduction in the heat of relaxation as a function of ageing time at room-temperature (i.e., ~0.69–0.70 $T_g$), as shown by the DSC curves in Fig. 2a and b, indicate that the glasses undergo a structural relaxation and move continuously towards lower levels of enthalpy.

The occurrence of a structural relaxation at room-temperature is confirmed by the DMA measurements (Fig. 3). In $Mg_{65}Cu_{25}Y_{10}$ and $Mg_{85}Cu_5Y_{10}$ the dominant behavior at room-temperature is solid-like since the values of the loss factor, $\tan\delta$, are very low, as shown in Fig. 3c. However, both glasses tend towards a more rigid configuration and lose part of the remaining liquid-like structure frozen in upon quenching, since $\tan\delta$ decreases further as a function of the ageing time. It should also be noted that $Mg_{65}Cu_{25}Y_{10}$ appears to be in a more rigid configuration

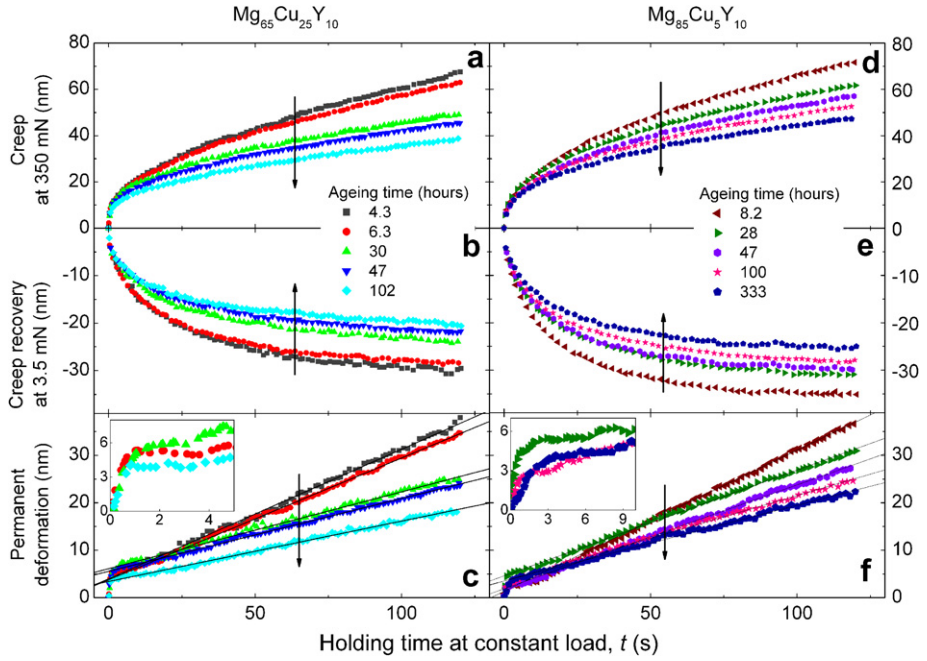


Fig. 5. Nanoindentation measurements at constant load for splat-cooled Mg-based samples aged at room-temperature for periods of between 4 and 333 h. Creep of (a) $Mg_{65}Cu_{25}Y_{10}$ and (d) $Mg_{85}Cu_5Y_{10}$ at 350 mN; creep recovery of (b) $Mg_{65}Cu_{25}Y_{10}$ and (e) $Mg_{85}Cu_5Y_{10}$ at 3.5 mN; permanent deformation of (c) $Mg_{65}Cu_{25}Y_{10}$ and (f) $Mg_{85}Cu_5Y_{10}$ during loading at 350 mN, obtained from the difference of the creep and creep recovery curves. The insets show the permanent deformations in the first 5–10 s.

than $Mg_{85}Cu_5Y_{10}$, since it shows lower values of $\tan\delta$. This may be due to the lower $T_g$ value of $Mg_{65}Cu_{25}Y_{10}$ in comparison to $Mg_{85}Cu_5Y_{10}$, which induces a slightly faster relaxation at room-temperature. However, the average values of $\tan\delta$ for $Mg_{65}Cu_{25}Y_{10}$ ($\sim$0.0015) and $Mg_{85}Cu_5Y_{10}$ ($\sim$0.007) normalized by the corresponding values of $T_{exp}/T_g$ (0.72 and 0.70, respectively) still show a lower value (0.002) for $Mg_{65}Cu_{25}Y_{10}$ than for $Mg_{85}Cu_5Y_{10}$ (0.01), meaning that the $Mg_{65}Cu_{25}Y_{10}$ glass (with the higher amount of the smallest atom Cu) has a more compact and, therefore, more rigid structure than $Mg_{85}Cu_5Y_{10}$.

As a consequence of ageing (i.e., structural relaxation), the deformation during creep at 350 mN and creep recovery at 3.5 mN decreases progressively with increasing ageing time, as shown in Fig. 5. The occurrence of a permanent deformation during the creep at 350 mN means that the deformation is not purely anelastic, as in the case of the recovery at 3.5 mN, but anelastic and viscoplastic (i.e., with time-dependent plastic deformation). Typically the viscoplastic deformation increases linearly with time during the hold at constant load, as shown by the linear fit in Fig. 5c and f. However, the beginning of the curves (see insets to Fig. 5c and f) shows a steeper part that deviates from this linear increase; this is probably a spurious effect due to the plastic deformation induced by the loading ramp. Similar behavior was reported in Ref. [34], where the amount of plastic deformation occurring in the constant load segment was found to increase with the loading rate. In fact, during loading increase at higher speeds there is not enough time to accommodate all the plastic deformation, and inhomogeneous plastic flow continues in the earlier stages of the holding segment. This means that the creep curves of the amorphous $Mg_{65}Cu_{25}Y_{10}$ and $Mg_{85}Cu_5Y_{10}$ samples need to be corrected by subtracting the plasticity induced by instantaneous deformation (i.e., deformation occurring during the first 1–2 s in Fig. 5c and f, respectively). The corrected creep curves are reported in Fig. 6a and c, together with the unchanged creep recovery curves (Fig. 6b and d).

Phenomenologically, the viscoelastic (anelastic and viscoplastic) deformation can be described as a series of linear springs and dashpots, known as the Kelvin model, which is commonly used for describing the creep of polymers [35], but can also be applied to metallic glasses (see e.g. [36]), i.e.

$$h = \sum_{i=1}^{n} h_i(1 - e^{-t/\tau_i}) + t/\mu_0 \qquad (2)$$

where $h_i$ is the indentation depth and $\tau_i$ is the characteristic relaxation time for the activation of the $i$-th anelastic process. In the second term on the right-hand side (r.h.s.) of Eq. (2), $t$ is the experimental time and $\mu_0$ is a constant proportional to the viscosity coefficient of the last dashpot. The anelastic deformation is a stress-induced relaxation phenomenon that obeys the kinetics described by the sum of exponential decays in the first term on the r.h.s. of Eq. (2). The viscoplastic contribution to the creep is represented by the second term.

The creep curves in Fig. 6a and c are successfully fitted by a series of two exponential decays, representing the anelastic deformation, plus the viscoplastic contribution $t/\mu_0$. The value of the viscoplastic term $\mu_0$, estimated from

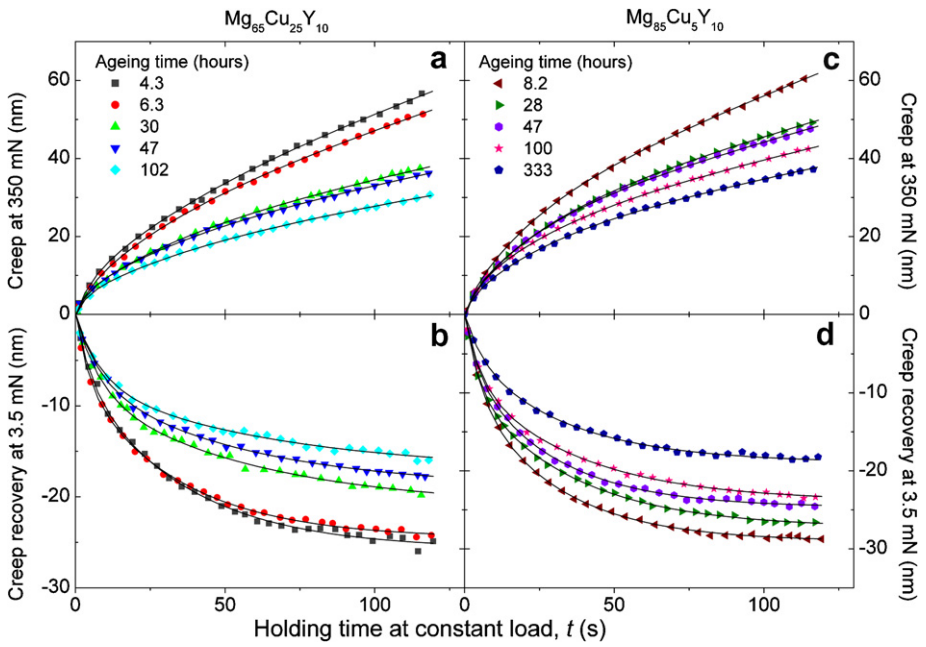


Fig. 6. Corrected creep curves (a and c) and creep recovery curves (b and d) of $Mg_{65}Cu_{25}Y_{10}$ and $Mg_{85}Cu_5Y_{10}$. The creep curves are fitted with the anelastic and viscoplastic terms of Eq. (2); the creep recovery curves are fitted only with the anelastic term of Eq. (2).

the slope of the linear fits in Fig. 5c and f, was inserted as a fixed parameter in the fitting procedure, leaving only $h_1$, $\tau_1$, $h_2$ and $\tau_2$ free to vary. The fit of the creep recovery curves does not take into account the viscoplastic term (Fig. 6b and d). The values of the fitting parameters for the creep curves, together with the error due to the fitting procedure, are reported in Table 2. The values of $h_1$ and $\tau_1$, describing the first component of the anelastic deformation, show no clear trend as a function of room-temperature ageing. However, the values of $h_2$ and $\tau_2$, associated with the second anelastic component, clearly change: while $h_2$ significantly decreases for both alloys, $\tau_2$ increases slightly with room-temperature ageing. Finally, $\mu_0$ increases with ageing because the viscosity rises progressively with structural relaxation.

It has been shown [37] that the number, the intensity and the characteristic relaxation time of the anelastic processes activated during the constant load segment depend on the loading time, the degree of structural relaxation and the temperature. In our case the interesting feature is the dependence on ageing time, which is proportional to the structural relaxation occurring at room-temperature. For $Mg_{65}Cu_{25}Y_{10}$ and $Mg_{85}Cu_5Y_{10}$ two anelastic deformation processes are activated during the holding segment at a homologous temperature ($T_{exp}/T_g$) of ~0.70. It is interesting to compare this result with that reported in Ref. [38] for $Pd_{40}Cu_{30}Ni_{10}P_{20}$, where only one anelastic deformation process is activated after the same holding time at $T_{exp}/T_g$ ~0.52. It is evident that a larger number of anelastic deformation processes is activated when the experiment is performed at higher reduced temperature $T_{exp}/T_g$.

The anelastic component of the creep can be analyzed in terms of a spectrum of relaxation times [39], and the isothermal relaxation spectra can be calculated by means of the following approximated expression [35]:

$$L(\tau) = \left[\sum_{i=1}^{n}\left(1+\frac{t}{\tau_i}\right)\frac{h_i}{\tau_i}e^{-t/\tau_i}\right]\frac{A_0}{P_0 h_{in}}t\Big|_{t=2\tau} \quad (3)$$

where $h_i$, $\tau_i$ and $t$ are the same parameters as in Eq. (2), $A_0/P_0$ is the inverse of the hardness $H$ and $h_{in}$ is the maximum indentation depth.

Table 2
Parameters from the fits of the creep curves in Fig. 6a and c, using Eq. (2)

| Alloy | Ageing time (h) | $h_1$ (nm) | $\tau_1$ (s) | $h_2$ (nm) | $\tau_2$ (s) | $\mu_0$ (s nm$^{-1}$) |
|---|---|---|---|---|---|---|
| $Mg_{65}Cu_{25}Y_{10}$ | 6.3 | 4.7 ± 0.3 | 4.8 ± 0.4 | 17.7 ± 0.2 | 34.0 ± 0.7 | 3.9 |
| | 30 | 4.0 ± 0.1 | 3.2 ± 0.2 | 15.3 ± 0.1 | 35.6 ± 0.6 | 6.2 |
| | 47 | 4.4 ± 0.2 | 3.3 ± 0.2 | 14.1 ± 0.1 | 36.0 ± 0.7 | 6.5 |
| | 102 | 4.1 ± 0.2 | 3.6 ± 0.3 | 11.8 ± 0.1 | 38.6 ± 1.1 | 7.9 |
| $Mg_{85}Cu_5Y_{10}$ | 8.2 | 2.9 ± 0.1 | 2.8 ± 0.2 | 22.8 ± 0.1 | 24.0 ± 0.2 | 3.3 |
| | 28 | 3.5 ± 0.1 | 2.8 ± 0.2 | 20.4 ± 0.1 | 27.2 ± 0.2 | 4.5 |
| | 47 | 2.7 ± 0.1 | 2.3 ± 0.2 | 20.0 ± 0.1 | 24.0 ± 0.2 | 4.6 |
| | 333 | 3.3 ± 0.1 | 2.9 ± 0.2 | 16.0 ± 0.1 | 27.8 ± 0.3 | 6.3 |

The viscoplasticity parameter $\mu_0$ was obtained independently from the linear fits of Fig. 5c and f.

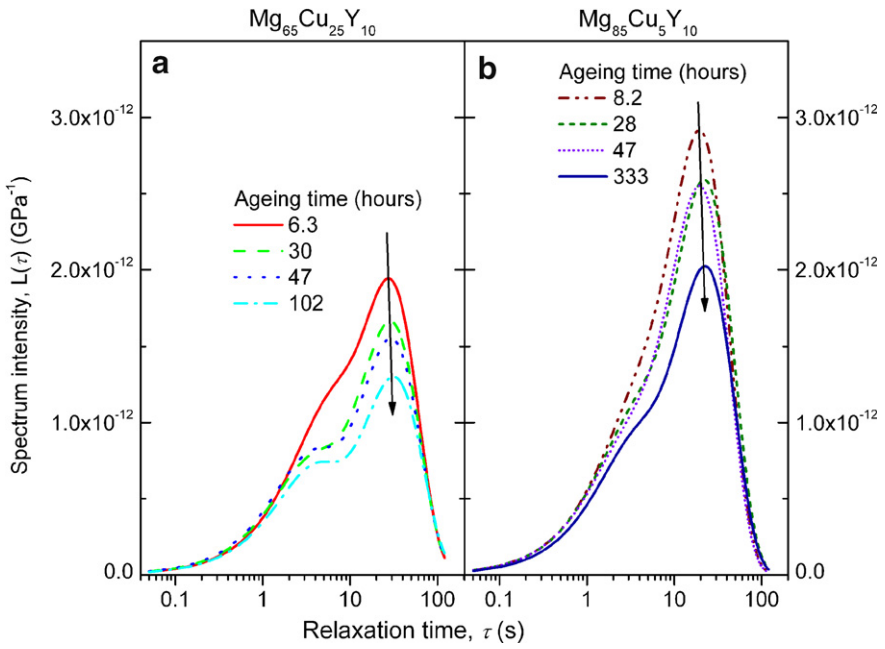


Fig. 7. Relaxation spectra of (a) $Mg_{65}Cu_{25}Y_{10}$ and (b) $Mg_{85}Cu_5Y_{10}$ calculated (see Eq. (3)) from the anelastic components of the creep curves in Fig. 6a and c, respectively.

Fig. 7 shows the spectra of splat-cooled $Mg_{65}Cu_{25}Y_{10}$ and $Mg_{85}Cu_5Y_{10}$. In the case of $Mg_{65}Cu_{25}Y_{10}$ the spectrum shows a progressive separation between the two peaks. Both peaks show a reduction in intensity and a shift towards longer relaxation times as the sample ages; such a trend is more pronounced for the second peak with respect to the first one. The reduction in the peak intensities and the shift of the peaks to longer relaxation times occur because the population of the corresponding defects decreases and the activation of the remaining defects becomes more difficult as structural relaxation proceeds.

The spectrum of $Mg_{85}Cu_5Y_{10}$ shows the same trend as for $Mg_{65}Cu_{25}Y_{10}$, but the distinction between the two peaks is less prominent and the intensity of the peaks, for the same ageing times, is higher than for $Mg_{65}Cu_{25}Y_{10}$. From this we may conclude that $Mg_{85}Cu_5Y_{10}$ is quenched to a less relaxed state than $Mg_{65}Cu_{25}Y_{10}$, in agreement with the DMA results shown in Fig. 3. This also explains the fact that $Mg_{85}Cu_5Y_{10}$ embrittles later than $Mg_{65}Cu_{25}Y_{10}$. In addition, the spectrum of $Mg_{85}Cu_5Y_{10}$ after 333 h of ageing at room-temperature shows the same shape and intensity as that of $Mg_{65}Cu_{25}Y_{10}$ after an ageing time of 6.3 h. This means that the two alloys are in a similarly relaxed state when they become fully brittle (see Fig. 1).

As mentioned earlier, each anelastic deformation process can be associated with the activation of localized shear transformations in weak regions of the glass involving small atomic clusters. Positron annihilation spectroscopy (PAS) measurements on $Mg_{65}Cu_{25}Y_{10}$ [27] reveal the presence of two different components for the positron lifetime that can be associated with small and large traps (defects), where positrons can be annihilated. Table 3 shows that the longer lifetime, corresponding to the larger defects, disappears after the sample has been stored at room-temperature for a period of 1–2 h, corresponding to the ageing time necessary for the embrittlement of the alloy. In contrast, the shorter lifetime component, associated with smaller defects, remains unchanged during the experiment. These findings also confirm earlier results obtained for a Zr-based BMG, where larger, thermally unstable defects are annihilated as a consequence of structural relaxation and small defects (intrinsic open-volume regions similar to Bernal interstitial sites) are not affected by relaxation [40].

Table 3
Positron lifetimes (LT) and corresponding intensities as a function of ageing time in $Mg_{65}Cu_{25}Y_{10}$ metallic glass

| Ageing time (h) | LT 1 (ps) | Intensity LT 1 (%) | LT 2 (ps) | Intensity LT 2 (%) |
|---|---|---|---|---|
| 0.003 | $0.224 \pm 0.002$ | 97.44 | $0.571 \pm 0.049$ | 2.56 |
| 0.005 | $0.223 \pm 0.002$ | 97.18 | $0.576 \pm 0.051$ | 2.82 |
| 0.012 | $0.216 \pm 0.003$ | 95.65 | $0.466 \pm 0.037$ | 4.35 |
| 0.033 | $0.211 \pm 0.004$ | 91.95 | $0.400 \pm 0.032$ | 8.05 |
| 0.083 | $0.219 \pm 0.002$ | 96.54 | $0.504 \pm 0.041$ | 3.46 |
| 0.33 | $0.222 \pm 0.002$ | 97.48 | $0.638 \pm 0.046$ | 2.52 |
| 1.3 | $0.222 \pm 0.001$ | 97.94 | $0.646 \pm 0.040$ | 2.06 |
| 7 | $0.222 \pm 0.002$ | 100 | – | 0 |
| 32 | $0.198 \pm 0.002$ | 100 | – | 0 |

According to Argon and co-workers [16,41], defects causing anelasticity and viscoplasticity are the same. When a load is applied all transformed volume elements are spatially isolated and do not touch each other during the earlier stage of deformation. As the deformation progresses with increasing strain, the probability grows that such transformed volume elements will become neighbors, with

a resulting clustering of adjacent elements. When the load is removed the memory of the initially unstressed state is lost such that these clustered regions can no longer undergo a reverse shear transformation, with the consequence that the material is deformed permanently by viscoplastic deformation. This picture can also apply to our case because only one type of defect (the large one) is affected by structural relaxation, but both anelastic and viscoplastic deformations decrease progressively as a consequence of room-temperature ageing.

Since anelastic deformation decreases with ageing time, we suggest that the larger defects observed by PAS are those primarily activated by localized shear transformation. This picture agrees well with that described in Ref. [14], where shear modes of vibration were uniquely attributed to the larger defects, while both large and small defects were presumed to contribute to the flexural modes. The activation of two distinct processes, characterized by two relaxation times, during the anelastic deformation (see Fig. 7) can be explained in terms of different stress fields surrounding the defects. The anelastic deformation tends to occur first in the volume elements characterized by a higher energy configuration (i.e., a lower degree of local relaxation) because of the lower activation energy required for the reversible transition from one configuration to another [41]. Finally, the disappearance of the long positron lifetime in accordance with the embrittlement of $Mg_{65}Cu_{25}Y_{10}$ suggests that a critical concentration of large defects is required for the formation of multiple shear bands, leading to macroscopic plasticity.

## 5. Conclusions

We have shown that ageing of splat-cooled $Mg_{65}Cu_{25}Y_{10}$ and $Mg_{85}Cu_5Y_{10}$ metallic glasses at room-temperature (corresponding to a homologous temperature $T/T_g$ of about 0.70) results in a sharp ductile-to-brittle transition upon bending due to structural relaxation. Dynamic mechanical analysis and nanoindentation measurements confirm that the relaxed samples are stiffer and harder than the as-quenched ones. In particular, the increase of storage modulus $E'$ and the decrease of loss modulus $E''$, together with the decrease in the internal friction $E''/E'$, show that the two amorphous alloys progressively lose the remaining liquid-like structure frozen in upon rapid quenching.

Nanoindentation creep curves show anelastic (recoverable) and viscoplastic (permanent) deformations. In the relaxation spectra, calculated from the anelastic components of creep, the peaks become progressively more distinct and show longer relaxation times and lower intensities with increasing aging time at room-temperature. This agrees with the picture of a progressive reduction of weak regions (or defects), where localized and reversible shear transformations can occur. The relaxation spectra also show that $Mg_{65}Cu_{25}Y_{10}$ is in a more relaxed state than $Mg_{85}Cu_5Y_{10}$ at similar ageing times, but that the two glasses are similarly relaxed when they transform to the fully brittle state (which occurs much later for the $Mg_{85}Cu_5Y_{10}$ glass).

Direct structural analysis using positron annihilation spectroscopy on the same specimens shows both small and large defects. While the small defects are unaffected by relaxation, the large ones are progressively annihilated during room-temperature ageing. The reduction of these defects, responsible for shear transformation, leads to an abrupt loss of plasticity and a continuous decrease in creep deformation.

## Acknowledgment

This work was financed by ETH Research Grant TH-21/04-2.

## References

[1] Greer AL. In: Liebermann HH, editor. Rapidly solidified alloys: process, structure, properties, applications. New York: Marcel Dekker; 1993. p. 269.
[2] Turnbull D, Cohen MH. J Chem Phys 1970;52:52.
[3] Slorovitz D, Maeda K, Vitek V, Egami T. Phil Mag A 1981;44:847.
[4] Argon AS. Acta Metall 1979;27:47.
[5] Bakai AS. In: Beck H, Güntherodt H-J, editors. Glassy metals III. Heidelberg: Springer; 1994. p. 209.
[6] Lewandowski JJ. Mater Trans 2001;42:633.
[7] Chi GC, Chen HS, Miller CE. J Appl Phys 1978;49:1715.
[8] Chen HS, Leamy HJ, Barmatz M. J Non-Cryst Solid 1971;13:321.
[9] Morito N, Egami T. Acta Mater 1984;32:603.
[10] Ashby MF, Greer AL. Scripta Mater 2006;54:321.
[11] Conner RD, Johnson WL, Paton NE, Nix WD. J Appl Phys 2003;94:904.
[12] Lewandowski JJ, Wang WH, Greer AL. Phil Mag Lett 2005;85:77.
[13] Gu XJ, McDermott AG, Poon SJ, Shiflet GJ. Appl Phys Lett 2006;88:211905.
[14] Castellero A, Uhlenhaut DI, Moser B, Löffler J. Phil Mag Lett 2007;87:383.
[15] Schroers J, Johnson WL. Phys Rev Lett 2004;93:255506.
[16] Argon AS. J Phys Chem Solid 1982;43:945.
[17] Murali P, Ramamurty U. Acta Mater 2005;53:1467.
[18] Raghavan R, Murali P, Ramamurty U. Intermetallics 2006;14:1051.
[19] van den Beukel A, van der Zwaag S, Mulder AL. Acta Metall 1984;32:1895.
[20] Kuršumović A, Cantor B. Scripta Mater 1996;34:1655.
[21] Gibbs MRJ, Sinning H-R. J Mater Sci 1985;20:2517.
[22] Khonik VA, Kosilov AT, Mikhailov VA, Sviridov VV. Acta Mater 1998;46:3399.
[23] Inoue A. Mater Trans JIM 1989;30:378.
[24] Zhang B, Wang RJ, Zhao DQ, Pan MX, Wang WH. Phys Rev B 2004;70:224208.
[25] Niikura A, Tsai AP, Inoue A, Masumoto T. J Non-Cryst Solid 1993;159:229.
[26] Yuan GY, Amiya K, Inoue A. J Non-Cryst Solid 2005;351:729.
[27] Uhlenhaut DI, Dalla Torre FH, Castellero A, Krauss G, Schmitt B, Patterson B, et al. Phys Rev B [submitted for publication].
[28] Oliver WC, Pharr GM. J Mater Res 1992;7:1564.
[29] Kim SG, Inoue A, Masumoto T. Mater Trans JIM 1990;31:929.
[30] Busch R, Liu W, Johnson WL. J Appl Phys 1998;83:4134.
[31] Yuan G, Zhang T, Inoue A. Mater Trans 2003;44:2271.
[32] Chen HS, Krause JT, Inoue A, Masumoto T. Scripta Metall 1983;17:1413.
[33] Zhang Y, Greer AL. J Alloys Compd 2007;434–435:2.

[34] Concustell A, Sort J, Alcalá G, Mato S, Gebert A, Eckert J, et al. J Mater Res 2005;20:2719.
[35] Ferry JD. Viscoelastic properties of polymers. 3rd ed. New York: John Wiley & Sons; 1980.
[36] Taub AI, Spaepen F. J Mater Sci 1981;16:3087.
[37] Ocelík V, Csach K, Kasardová A, Bengus VZ. Mater Sci Eng A 1997;226–228:851.
[38] Concustell A, Sort J, Greer AL, Baró MD. Appl Phys Lett 2006;88:171911.
[39] Primak W. Phys Rev 1955;100:1677.
[40] Suh D, Dauskardt RH, Asoka-Kumar P, Sterne PA, Howell RH. J Mater Res 2003;18:2021.
[41] Argon AS, Shi LT. Acta Metall 1983;31:499.